Discovery of a Basaltic Asteroid in the Outer Main Belt

D. Lazzaro *et al.*

Science **288**, 2033 (2000);
DOI: 10.1126/science.288.5473.2033

Science (print ISSN 0036-8075; online ISSN 1095-9203) is published weekly, except the last week in December, by the American Association for the Advancement of Science, 1200 New York Avenue NW, Washington, DC 20005.

from 90 to no more than 140 mW cm^{-2} as thickness decreased from 0.5 to 0.15 mm.

The partial oxidation of ethane represented by Eq. 1 is thermodynamically possible even below 773 K:

$$C_2H_6 + O_2 \rightarrow 3H_2 + 2CO$$
$$\Delta G°(673\ K) = -383\ kJ\ mol^{-1} \quad (7)$$

where $\Delta G°$ is Gibbs free energy. We therefore studied the performance of the single-chamber SOFC using SDC with a thickness of 0.15 mm under such conditions (Fig. 5). In the range of 623 to 723 K, the cell generated EMFs of ~900 mV, and the discharge properties were stable and reproducible. No carbon deposition was observed on the anode after operation. In addition, the impedance spectra of the cell showed small electrode-reaction resistances: 0.34 ohms for 723 K, 0.79 ohms for 673 K, and 1.64 ohms for 623 K. It appears that such fast electrode kinetics clean the precursors for carbon formation on the anode.

Figure 5 also shows the corresponding results for the other hydrocarbons. The cell performance in a mixture of propane and air was similar to that in a mixture of ethane and air, except at 723 K, where the $Sm_{0.5}Sr_{0.5}CoO_3$ electrode could not function well as the cathode, because this material was no longer inert to the oxidation of propane. On the other hand, the EMFs generated from the cell in a mixture of methane and air were only ~120 mV throughout the tested temperature range, where the oxidation rate of methane was too slow to form hydrogen and carbon monoxide over the 10 weight % SDC–containing Ni anode, probably causing a depression in Eqs. 2 and 3. We thus conclude that ethane and propane can be successfully used in the present SOFC at an operating temperature of 773 K or less. Because of their similar properties, we can assume that liquefied petroleum gas (LPG) or even butane would perform equally well.

The present SOFC has several additional advantages over PEFCs: (i) The anode is not subject to poisoning by carbon monoxide, whereas it is a critical problem for PEFCs (*15, 16*). (ii) There is no noble metal, such as Pt, in our SOFC, so fabrication costs are low. (iii) Although PEFCs themselves can operate at low temperatures, the hydrocarbon reformer (*17*) must operate at a higher temperature than our SOFC. (iv) The single-chamber cell design provides a more compact cell stack. These advantages, as well as the above results, greatly enhance the position of SOFCs as the preferred electric power generation technique for vehicles in the foreseeable future.

References

1. E. P. Murray, T. Tsai, S. A. Barnett, *Nature* **400**, 649 (1999).
2. S. Park, J. M. Vohs, R. J. Gorte, *Nature* **404**, 265 (2000).
3. W. van Gool, *Philips Res. Rep.* **20**, 81 (1965).
4. G. A. Lousi, J. M. Lee, D. L. Maricle, J. C. Trocciola, U.S. Patent 4,248,941 (1981).
5. C. K. Dyer, *Nature* **343**, 547 (1990).
6. T. Hibino and H. Iwahara, *Chem. Lett.*, 1131 (1993).
7. C. A. Cavalca, G. Larsen, C. G. Vayenas, G. L. Haller, *J. Phys. Chem.* **97**, 6115 (1993).
8. I. Riess, P. J. van der Put, J. Schoonman, *Solid State Ionics* **82**, 1 (1995).
9. T. Hibino, S. Wang, S. Kakimoto, M. Sano, *Electrochem. Solid-State Lett.* **2**, 317 (1999).
10. B. C. H. Steele, *J. Power Source* **49**, 1 (1994).
11. C. Milliken, S. Guruswamy, A. Khandkar, *J. Electrochem. Soc.* **146**, 872 (1999).
12. H. L. Tuller and A. W. Nowick, *J. Electrochem. Soc.* **122**, 255 (1975).
13. A. T. Ashcroft *et al.*, *Nature* **344**, 319 (1990).
14. H. Uchida, M. Yoshida, M. Watanabe, *J. Phys. Chem.* **99**, 3282 (1995).
15. S. Mukerjee *et al.*, *Electrochem. Solid-State Lett.* **2**, 12 (1999).
16. M. Ciureanu and H. Wang, *J. Electrochem. Soc.* **146**, 4031 (1999).
17. N. Hashimoto, *Chem. Chem. Ind.* **50**, 1324 (1997).

28 February 2000; accepted 1 May 2000

Discovery of a Basaltic Asteroid in the Outer Main Belt

D. Lazzaro,[1]* T. Michtchenko,[2] J. M. Carvano,[1] R. P. Binzel,[3] S. J. Bus,[3] T. H. Burbine,[3] T. Mothé-Diniz,[1] M. Florczak,[4] C. A. Angeli,[1] Alan W. Harris[5]

Visible and near-infrared spectroscopic observations of the asteroid 1459 Magnya indicate that it has a basaltic surface. Magnya is at 3.15 astronomical units (AU) from the sun and has no known dynamical link to any family, to any nearby large asteroid, or to asteroid 4 Vesta at 2.36 AU, which is the only other known large basaltic asteroid. We show that the region of the belt around Magnya is densely filled by mean-motion resonances, generating slow orbital diffusion processes and providing a potential mechanism for removing other basaltic fragments that may have been created on the same parent body as Magnya. Magnya may represent a rare surviving fragment from a larger, differentiated planetesimal that was disrupted long ago.

The diversity of compositions of iron meteorites and nonchondritic stony meteorites (*1*) suggests an early period of heating, melting, and differentiation of planetesimals that were later disrupted and became asteroids in the main belt rather than accreting to form planets. In the main belt today, only the large (525-km diameter) asteroid Vesta (*2–4*) and its associated family of impact excavated fragments (*5–9*) have been considered to be basaltic remnants (representing the crust of a differentiated planetesimal) from this early epoch of solar system history. We report observations of a 30-km outer main-belt asteroid, 1459 Magnya, that also shows the characteristic signature of a basaltic surface.

In September 1998, we performed spectroscopic observations of Magnya that indicated its possible basaltic composition (*10*) at the European Southern Observatory at La Silla (ESO-Chile) (*11*). Additional observations of this asteroid were obtained in November 1999 and January 2000 with the double spectrograph on the 5-m Hale telescope at Palomar Observatory and in December 1999 with NSFCAM on the 3-m NASA Infrared Telescope Facility (IRTF) at Mauna Kea, Hawaii (*12*).

The ESO, Palomar, and Mauna Kea spectra of Magnya compared with the spectra of Vesta (Fig. 1) show similar absorptions near 1 and 2 μm, indicating a basaltic composition for Magnya. The basaltic nature of these surfaces is further confirmed by their match to basaltic achondrite meteorites, such as meteorites from the howardite, eucrite, and diogenite (HED) classes. Although Vesta has been suggested as a source for HED meteorites (*7–9*, *13*), the implied ejection velocity (*7*, *8*) for a fragment the size of Magnya being ejected from Vesta (at semimajor axis, a, of 2.36 AU) to Magnya's present location (a = 3.14 AU, e = 0.24, and i = 17°, where e and i are the orbit eccentricity and inclination, respectively) is in excess of 5 km/s. We consider this high velocity to exceed any plausible limit for linking Magnya as a fragment directly ejected from Vesta. The orbits of Magnya and Vesta do overlap (the perihelion distance of Magnya is less than the aphelion distance of Vesta), leaving open some possibility that Magnya is an ejected and dynamically evolved fragment from Vesta. However, the lack of other evidence for such a dynamical evolution of the Vesta family (*5–8*) makes this link unlikely. Therefore, we consid-

[1]Observatório Nacional, Departamento de Astrofísica, Rua Gal. José Cristino 77, 20921-400 Rio de Janeiro, Brazil. [2]Instituto Astronômico e Geofísico, Universidade de São Paulo, Av. Miguel Stefano 4200, 04301-904 São Paulo, Brazil. [3]Department of Earth, Atmospheric, and Planetary Sciences, Massachusetts Institute of Technology, 77 Massachusetts Avenue, Cambridge, MA 02139–4301, USA. [4]Centro Federal de Educacão Tecnológica do Paraná, Departamento de Física, Av. Sete de Setembro 3165, 80230-901 Curitiba, Brazil. [5]Jet Propulsion Laboratory, MS 183-501, 4800 Oak Grove Drive, Pasadena, CA 91109, USA.

*To whom correspondence should be addressed.

er the case that Magnya represents a sample of an independently formed basaltic asteroid, making it the only known main-belt basaltic asteroid residing beyond Vesta and the region of the Vesta family.

The albedo of 1459 Magnya was measured by the Infrared Astronomical Satellite (IRAS), and its calibrated albedo and diameter are 0.12 ± 0.03 and 30 km, respectively (*14*). This albedo is different from the 0.42 ± 0.05 value for Vesta, although Vesta displays a range of albedos over its surface and even the darker regions retain their basaltic spectral signature (*4*, *15*). Magnya was at the limit of IRAS's detectability (registering in only one of four potential sightings) and was located in a region containing a high concentration of background objects at the time of detection. Imposing Vesta's albedo on Magnya would reduce its calculated size to 15 km. This smaller size is at the limit for the suggested thickness of a basaltic crust formed on a thoroughly heated and differentiated Vesta-like asteroid (*16*, *17*) but exceeds the upper size range (10-km diameter) of basaltic asteroids recognized in the vicinity of Vesta (*7*, *8*). The tabulated 30-km size for Magnya would imply either that it is a conglomeration of basaltic fragments from a disrupted Vesta-like body or that its basaltic signature is the result of a different heating and melting history (*18*).

To test the hypothesis that Magnya is a collisional remnant of a large differentiated parent body, we looked for evidence of a nearby dynamical family that would be the natural outcome of a catastrophic disruption. The nearest family in this region is that of 137 Meliboea (*6*). However, plotting the proper elements of Milani and Knezević (*19*) for this family shows that it is concentrated at a mean proper a of 3.10 to 3.11 AU, with no apparent extension that would include 1459 Magnya at 3.15 AU. Furthermore, the C-type taxonomic classification of Meliboea (*14*), interpreted to be analogous to relatively unheated carbonaceous chondrite meteorites, is incompatible with the basaltic composition of Magnya being related to basaltic achondrites that formed under different pressure and temperature conditions. On a small sample of available asteroids with known composition, there is some possible evidence of a greater number of objects with an inferred composition compatible with the breakup of a differentiated body in the proximity of Magnya than in the neighboring regions. Magnya may also be the remnant of a catastrophic disruption in which most of the other fragments were ejected from this region.

We performed a precise numerical integration of test particles, accounting for the perturbations due to the four jovian planets. The initial conditions of the test particles were uniformly distributed in the ranges a = 3.13 to 3.18 AU (Δa = 0.001 AU), e = 0.14 to 0.32 (Δe = 0.005), and i = 14° to 24° (Δi = 0.5°). The orbital paths obtained over 1.5 million years (My) were Fourier-transformed, and the spectral number N associated with each initial condition used was defined as the number of substantial (more than 10% of the largest peak) spectral peaks in the asteroid semimajor axis oscillation. Large values of N (>40) indicate the onset of chaos (*20*).

The orbital dynamics in the region around Magnya is affected by two mean-motion resonances with Jupiter, namely 17:8 and 19:9, and five three-body resonances with Jupiter and Saturn, namely 6:1:−3, 8:−4:−3, 3:3:−2, 5:−2:−2, and 7:−2:−3 (*21*) (Fig. 2). All mean-motion resonances generate chaos with a maximum Lyapunov exponent larger than $10^{-4.5}$ year^{-1} and are responsible for enhancement of the orbital diffusion speed of asteroids in this region (*22*). Magnya is close to the $g + s - g_5 - s_7$ secular resonance, where g and s are the asteroid's perihelion and node frequencies, respectively, and g_5 and s_7 are two of the secular planetary frequencies (*19*) (Fig. 2).

We numerically integrated the evolution

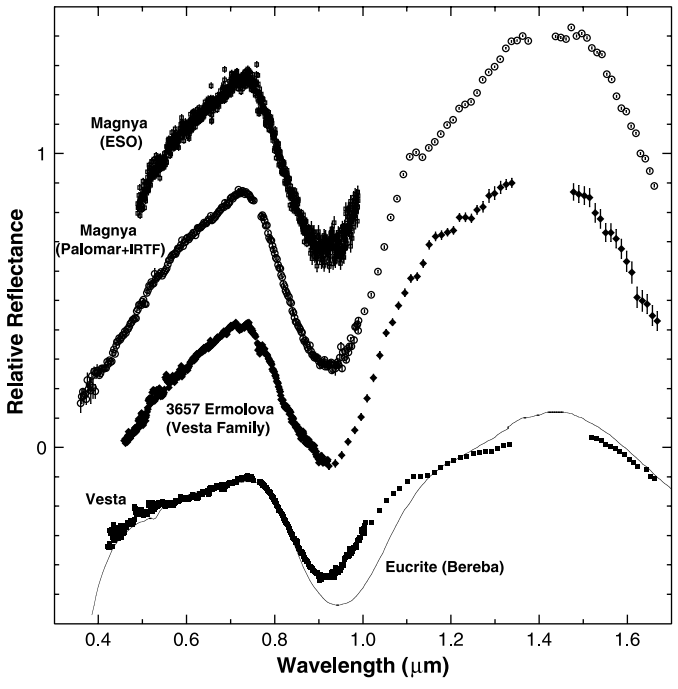

Fig. 1. The discovery spectrum of asteroid 1459 Magnya is displayed at top with the follow-up spectrum confirming its basaltic signature displayed immediately below. For comparison, we show the similar spectra of Vesta family asteroid 3657 Ermolova and 4 Vesta (*26*) and the spectrum for a typical eucrite (Bereba) meteorite (*27*). All spectra are normalized to unity at 0.55 μm, and all asteroid spectra are offset vertically by 0.2 for clarity.

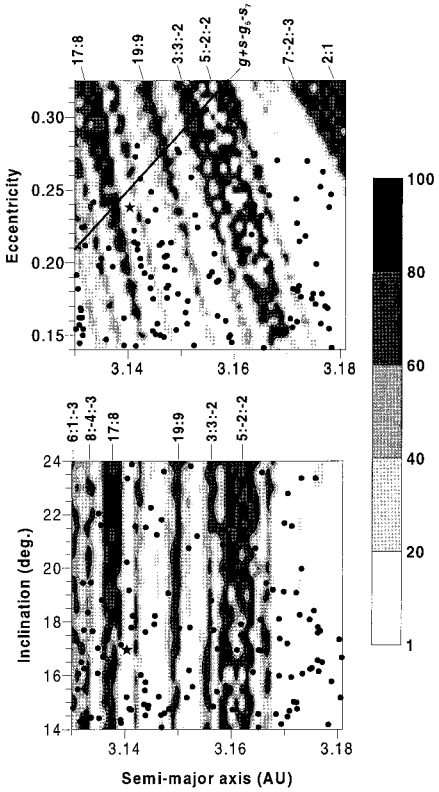

Fig. 2. Dynamical maps of the region around 1459 Magnya. The values of the spectral number N obtained in the range from 1 to 80 are coded by gray levels that vary linearly from white (N = 1) to black (N = 80) and plotted on the (a,e) (**top**) and (a,i) (**bottom**) planes of initial osculating orbital elements. The lighter regions indicate regular motion, whereas the darker regions indicate chaotic motion. The initial values of inclination (bottom), eccentricities (top), and angular elements of the test particles were chosen to be equal to those of Magnya. The location of mean-motion resonances is indicated by the combination of integers k:l:m or k:m. The border of the 2:1 asteroidal mean-motion resonance with Jupiter appears at the top right corner in the top panel. The $g + s - g_5 - s_7$ secular resonance is plotted by the solid line. The symbol ⋆ represents the position of 1459 Magnya. The distribution of the actual asteroids (●) in the region around Magnya, according to the 1998 version of Bowell's data base (JD2451100.5) (*28*), is presented.

of the orbit of Magnya subjected to the perturbations of the jovian planets for 70 My. Magnya is not presently involved in any resonance, and its motion is regular over the computed time span. The long-term behavior of the characteristic angle of the $g + s - g_5 - s_7$ secular resonance is a prograde circulation with a period ~ 1.37 My. The proximity of the asteroid to the secular resonance involving the longitudes of the perihelion and of the node affects the asteroid's e and i and may explain their high values.

About 200 asteroids have been observed in the Magnya region, and about 20 of these asteroids are presently involved in some mean-motion resonances showing chaotic behavior. The majority of the actual asteroids appear to avoid the chaotic domains that indicate the possible existence of important diffusion processes associated with the mean-motion resonances.

Our spectra and orbital dynamic simulations suggest that after the breakup of Magnya's parent body, the fragments were scattered around a wide region depending on physical parameters such as the impact energy and the strength of the parent body and the sizes and velocities of the ejected fragments. The fragments that fell into the chaotic zones were slowly diffused out of the region, whereas Magnya, and possibly some other fragments, remained in stable orbits outside the zones of chaotic motion.

Geochemical data imply that the HEDs are derived from a single parent body (*16*, *17*). The spectral evidence and the abundance of apparent Vesta fragments in the resonance-rich inner solar system suggest that Vesta is the HED parent body (*2*–*9*). However, the transport time of main-belt asteroids to near-Earth space through the 3:1 and ν_6 resonances is of shorter duration than the cosmic ray exposure time of meteorites. Although slower diffusion processes such as a multitude of weak resonances (*23*–*25*) may solve this problem for all meteorite types including the HEDs, fragments from the Magnya parent body would also have long exposure times. However, considering our current understanding of the much lower delivery efficiency from the outer belt relative to the inner belt, we do not consider Magnya to be a likely alternative source to Vesta for the HED meteorites.

References and Notes

1. J. T. Wasson and G. W. Wetherill, in *Asteroids*, T. Gehrels, Ed. (Univ. of Arizona Press, Tucson, AZ, 1979), pp. 926–974.
2. T. B. McCord, J. B. Adams, T. V. Johnson, *Science* **168**, 1445 (1970).
3. L. A. McFadden, T. B. McCord, C. Pieters, *Icarus* **31**, 439 (1977).
4. R. P. Binzel *et al.*, *Icarus* **128**, 95 (1997).
5. J. G. Williams, in *Asteroids II*, R. P. Binzel, T. Gehrels, M. S. Matthews, Eds. (Univ. of Arizona Press, Tucson, AZ, 1989), pp. 1034–1072.
6. V. Zappalà, P. Bendjoya, A. Cellino, P. Farinella, C. Froeschlé, *Icarus* **116**, 291 (1995).
7. R. P. Binzel and S. Xu, *Science* **260**, 186 (1993).
8. T. H. Burbine and R. P. Binzel, *Bull. Am. Astron. Soc.* **29**, 964 (1997).
9. P. C. Thomas *et al.*, *Science* **277**, 1492 (1997).
10. D. Lazzaro, C. A. Angeli, M. Florczak, M. A. Barucci, M. Fulchignoni, *Bull. Am. Astron. Soc.* **29**, 975 (1997).
11. The observations were obtained at the ESO (La Silla, Chile) under an agreement with the Conselho Nacional de Desenvolvimento Científico e Tecnológico (CNPq)–Observatório Nacional (Brazil). We used the 1.52-m telescope equipped with a Boller and Chivens spectrograph and a charge-coupled device (CCD) (2048 × 2048 pixels) with a readout noise of ±7 electrons and a grating of 225 grooves/mm, with a dispersion of 330 Å/mm in the first order. The CCD has a square 15-μm pixel, giving a dispersion of about 5 Å/pixel in the wavelength direction. The useful spectral range is about $4900 < \lambda < 9200$ Å with a full width at half maximum of 10 Å. The spectra were taken through a 5-arc sec slit oriented in the east-west direction. The spectral data reduction was performed with the IRAF package and the classical procedure with averaged bias and flat fields, wavelength calibration with a He-Ar lamp (obtained several times during each night), and correction from air mass with the mean extinction curve of La Silla.
12. The instrumentation and observing procedures are described by S. J. Bus *et al.* (in preparation). Both instruments are long-slit grism spectrographs that use CCD array detectors providing about 30 arc sec of spatial resolution over their full range of spectral sensitivity. The spectrum of the sky background is recorded simultaneously with that of the object. Sky subtraction and spectral summing were accomplished with the IRAF package produced by the National Optical Astronomical Observatories.
13. F. Migliorini *et al.*, *Meteorit. Planet. Sci.* **32**, 903 (1997).
14. E. F. Tedesco, Planetary Data System—Small Bodies Node (PDSSBN), M. A'Hearn (University of Maryland, College Park, MD) (available at pdssbn.astro.umd.edu).
15. B. H. Zellner *et al.*, *Icarus* **128**, 83 (1997).
16. M. J. Drake, in *Asteroids*, T. Gehrels, Ed. (Univ. of Arizona Press, Tucson, AZ, 1979), pp. 765–782.
17. G. J. Consolmagno and M. J. Drake, *Geochim. Cosmochim. Acta* **41**, 1271 (1977).
18. E. R. D. Scott *et al.*, in *Asteroids II*, R. P. Binzel, T. Gehrels, M. S. Matthews, Eds. (Univ. of Arizona Press, Tucson, AZ, 1989), pp. 701–739.
19. A. Milani and Z. Knezević, *Icarus* **107**, 219 (1994).
20. T. A. Michtchenko and S. Ferraz-Mello, *Astron. Astrophys.* **303**, 945 (1995).
21. The three-body mean-motion resonances involve the mean motions of Jupiter, Saturn, and the asteroid, $\mathbf{n}_{Jup}$, $\mathbf{n}_{Sat}$ and $\mathbf{n}$, respectively, which obey the relation $k\mathbf{n}_{Jup} + l\mathbf{n}_{Sat} + m\mathbf{n} \sim 0$, where k, l, and m are integers (*23*, *24*).
22. D. Nesvorný and A. Morbidelli, *Astron. J.* **116**, 3029 (1998).
23. A. Morbidelli and D. Nesvorný, *Icarus* **139**, 295 (1999).
24. P. Farinella and D. Vokrouhlicky, *Science* **283**, 507 (1999).
25. ———, W. K. Hartmann, *Icarus* **132**, 378 (1998).
26. T. H. Burbine, thesis, Massachusetts Institute of Technology, Cambridge, MA (2000).
27. M. J. Gaffey, *J. Geophys. Res.* **81**, 905 (1976).
28. E. Bowell, K. Muinonen, L. H. Wasserman, *IAU Symp.* **160**, 477 (1994).

29. The Brazilian authors gratefully acknowledge the support of CNPq, Fundacão de Amparo à Pesquisa do Estado de São Paulo, Fundacão de Amparo à Pesquisa do Estado de Rio de Janeiro, and Fundacão Coordencão de Aperfeic de Pessoal de Nível Superior through diverse grants and fellowships and the Computation Center of the University State of São Paulo (LCCA-USP). The Massachusetts Institute of Technology portion of this research was supported by NASA grant NAG5-3939 and NSF grant AST-9530282.

23 February 2000; accepted 20 April 2000

Hierarchical Self-Assembly of F-Actin and Cationic Lipid Complexes: Stacked Three-Layer Tubule Networks

Gerard C. L. Wong,[1]* Jay X. Tang,[2]† Alison Lin,[1] Youli Li,[1] Paul A. Janmey,[2]‡ Cyrus R. Safinya[1]§

We describe a distinct type of spontaneous hierarchical self-assembly of cytoskeletal filamentous actin (F-actin), a highly charged polyelectrolyte, and cationic lipid membranes. On the mesoscopic length scale, confocal microscopy reveals ribbonlike tubule structures that connect to form a network of tubules on the macroscopic scale (more than 100 micrometers). Within the tubules, on the 0.5- to 50-nanometer length scale, x-ray diffraction reveals an unusual structure consisting of osmotically swollen stacks of composite membranes with no direct analog in simple amphiphilic systems. The composite membrane is composed of three layers, a lipid bilayer sandwiched between two layers of actin, and is reminiscent of multilayered bacterial cell walls that exist far from equilibrium. Electron microscopy reveals that the actin layer consists of laterally locked F-actin filaments forming an anisotropic two-dimensional tethered crystal that appears to be the origin of the tubule formation.

Self-assembly of amphiphilic molecules constitutes one of the most fundamental mechanisms for the construction of soft condensed matter materials. The distinct geometries adapted by lipids are typically described within a consistent framework of continuum elastic